Supplementary Information

Textile-integrated multilayer liquid metal soft circuits for multienvironment wearable electronics

Brittan T. Wilcox[1], Ella T. Williams[1], and Michael D. Bartlett[1,2*]

[1]Mechanical Engineering, Soft Materials and Structures Lab, Virginia Tech, Blacksburg, VA 24061, USA.

[2]Macromolecules Innovation Institute, Virginia Tech, Blacksburg, VA 24061, USA.

*Corresponding author email: mbartlett@vt.edu

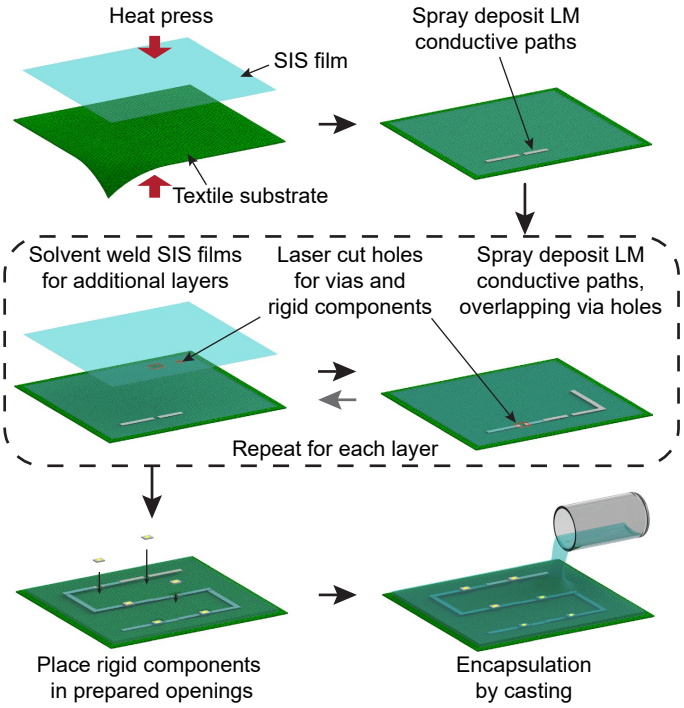

Fig. S1 Steps of the fabrication process to create textile-integrated LM soft circuits.

Supplier Part Number	Weight	Material	Weave	Coating
Rockywoods RBC200-Bright Orange	200 Denier	Polyester	Packcloth / Single Ply	C0 DWR and PU
Rockywoods RBC400-Coyote Brown	400 Denier	Polyester	Packcloth / Single Ply	C0 DWR and PU
Rockywoods RBC600-Black Knight	600 Denier	Polyester	Packcloth / Single Ply	C0 DWR and PU
Rockywoods CORDURAPOLY-White	1000 Denier (915 x 1220 Denier)	Polyester	Cordura	DWR and PU (Cordura)
Rockywoods P6603-Royal Purple	200 Denier (3.2 oz/ yard^2)	Polyester	Oxford	DWR PU
Rockywoods 6603-Burgundy	200 Denier (3.0-3.5 oz/yard^2)	Nylon	Oxford	DWR Polyurethane
Fabric Wholesale Direct SV578446	90-93 g/m^2	90% Polyester 10% Spandex	"Dricloth" Microfiber Jersey (Athletic Mesh Jersey)	none
Fabric Wholesale Direct SV571140	240 g/m^2	95% Polyester 15% Spandex	Knit Jersey Interlock twist yarn (Spandex)	none
Fabric Wholesale Direct SV573752	200 g/m^2	80% Nylon 20% Spandex	Tricot (Spandex)	none
Fabric Wholesale Direct SV573678	180 g/m^2	95% Cotton 5% Spandex	Jersey (T-shirt)	none
Fabric Wholesale Direct SV577954	268 g/m^2	Cotton	Twill	none
Fabric Wholesale Direct SV577937	156 g/m^2	Cotton	Twill	none

Table 1: Fabric suppliers and specifications

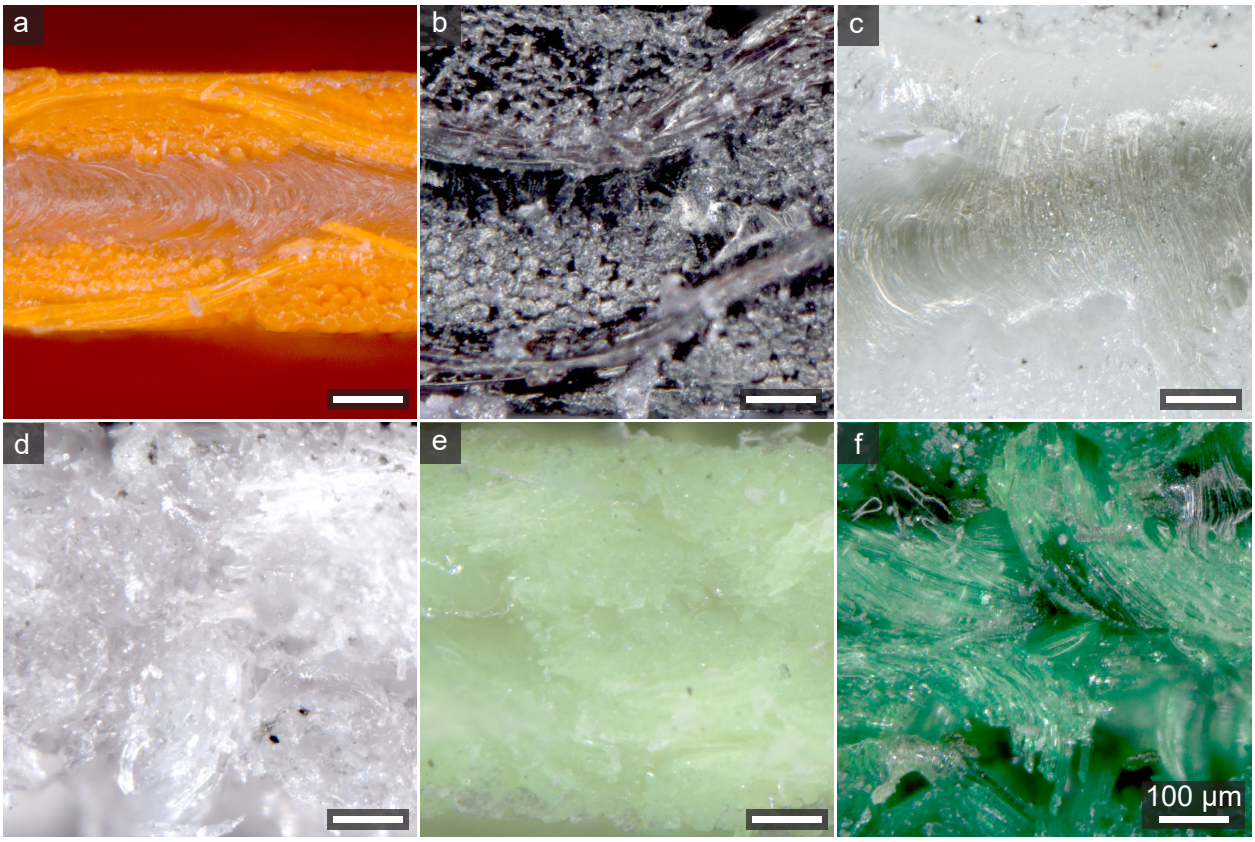

Fig. S2 Detailed images of SIS bonded textiles. Top row shows polyesters of increasing deniers: (a) 200D polyester, (b) 600D, and (c) 1000D. Bottom row shows various non-coated fabrics: (d) 156 g/m^2 cotton, (e) athletic mesh, and (f) polyester spandex.

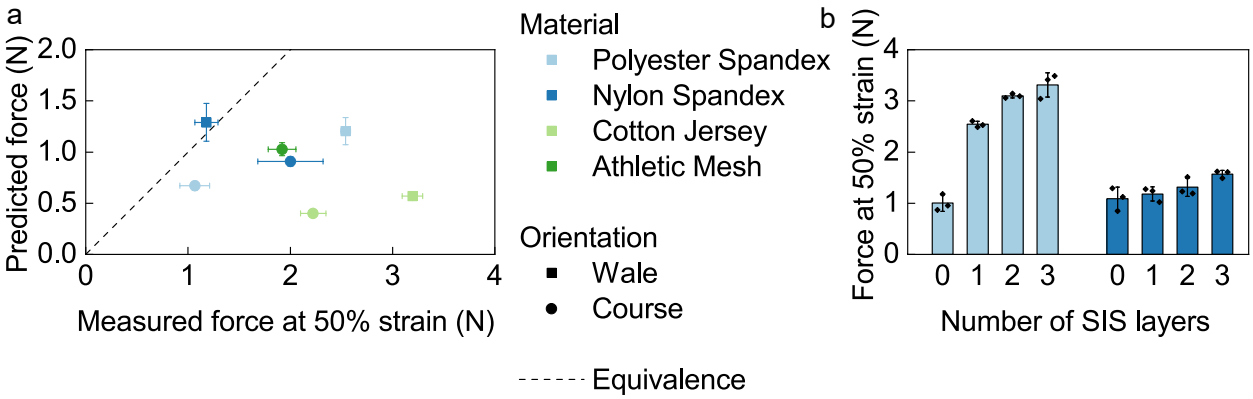

Fig. S3 Contribution of SIS layers to elastomer-embedded textile stiffness. (a) Comparison of the sum of the forces required to strain independent layers of textile and SIS in parallel ("Predicted force," $Predicted\ force = force_{\ textile} + force_{\ SIS}$) to $\epsilon = 50\%$ versus the force required to extend textile-SIS fully integrated through heat press processing to $\epsilon = 50\%$ ("Measured force at 50% strain"). Most textiles show a dramatic increase in stiffness. The exception is nylon spandex in the wale direction. (b) Force required to to strain polyester and nylon spandex textiles with 0, 1, 2, and 3 layers of SIS to $\epsilon = 50\%$ in the wale direction.

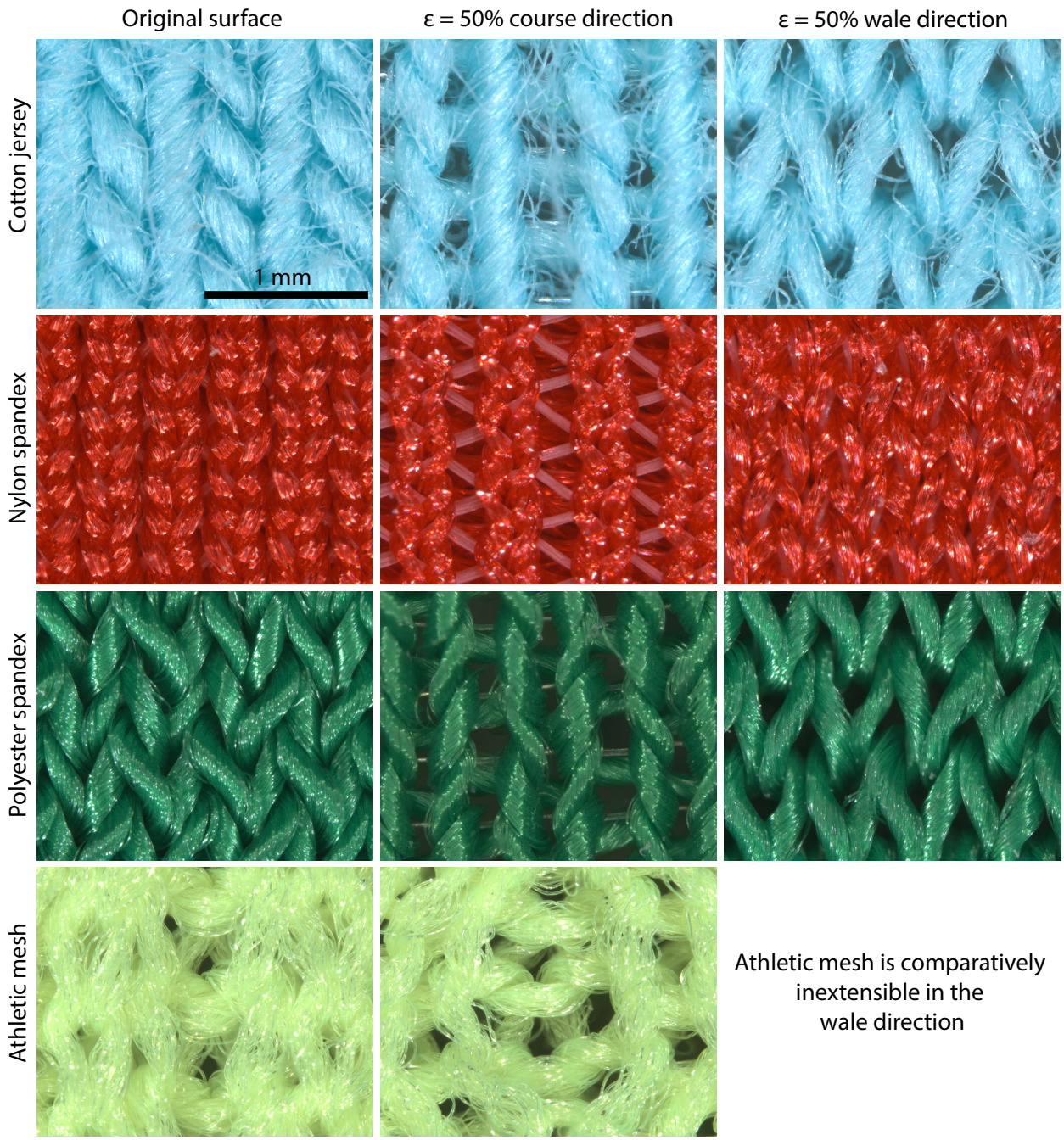

Fig. S4 Microscopy of extensible fabric surfaces. Note that most textiles display an opening behavior under strain, with the exception of the nylon spandex in the wale direction possibly explaining the close agreement with a parallel springs model

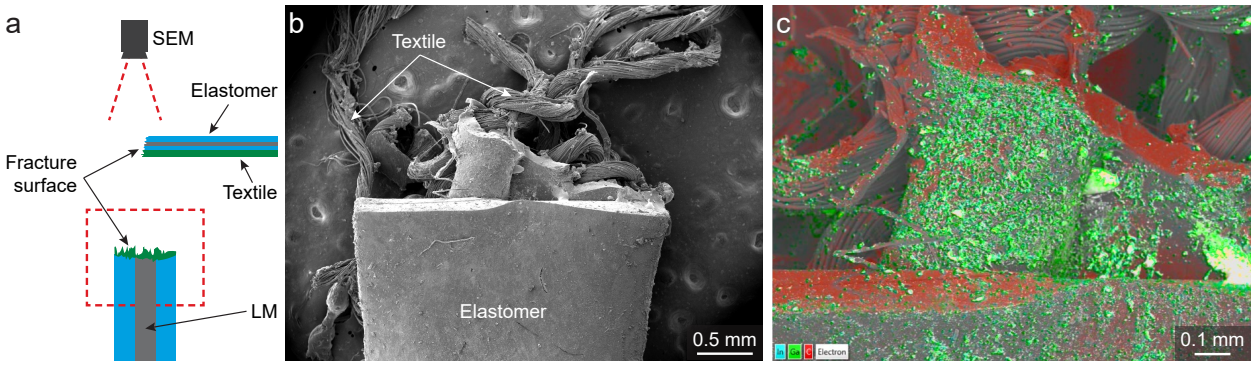

Fig. S5 Scanning Electron Microscopy (SEM) of fracture. (a) Schematic of specimen orientation in SEM imaging. (b) SEM image of fracture surface of a SIS-LM wire on spandex test specimen. (c) SEM energy dispersive X-ray spectroscopy (EDS) analysis of the fracture surface.

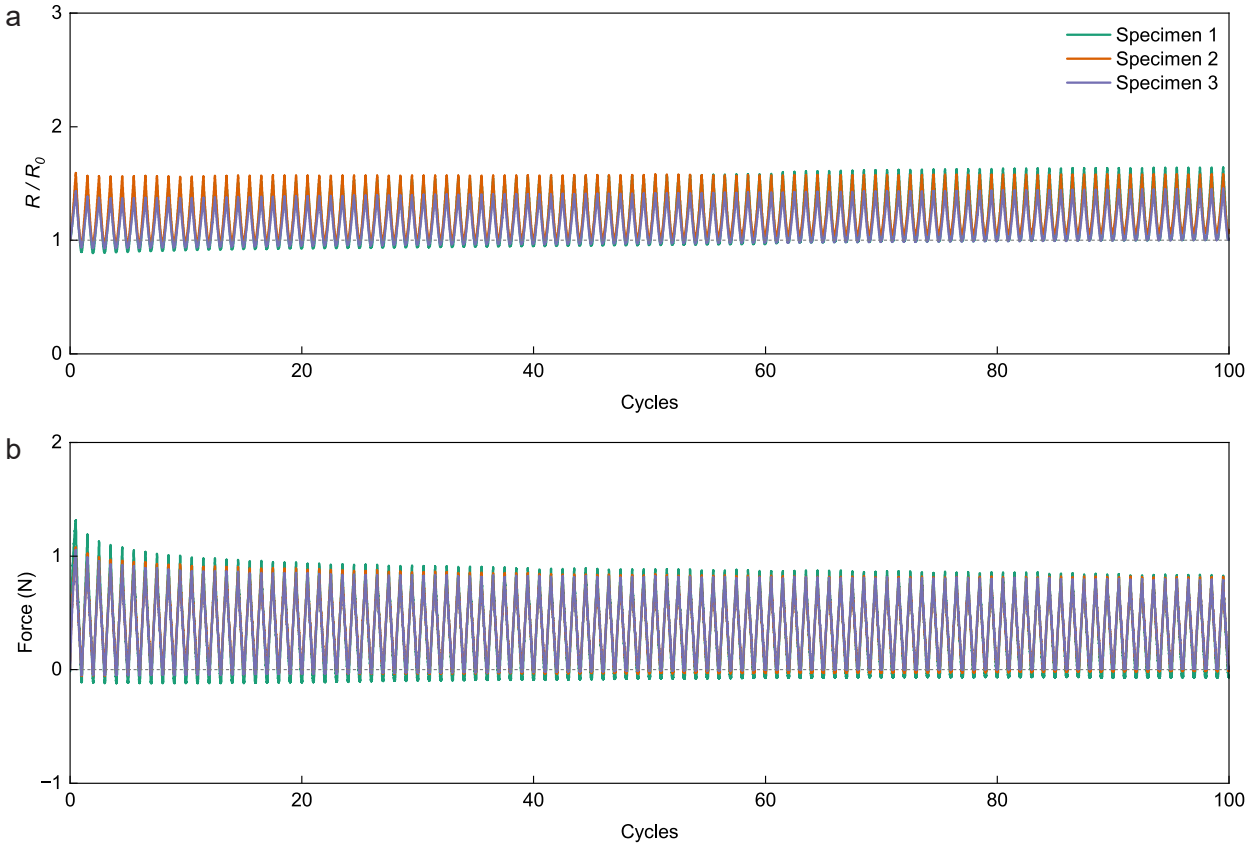

Fig. S6 Electromechanical characterization under cyclic tensile loading. (a) Normalized resistance of SIS-LM wires on spandex for cyclic tensile loading to 25% strain at 60 mm/min. Sample layout is the same as depicted in the inset of Figure 4a. (b) Force over time for same specimens as in (a).

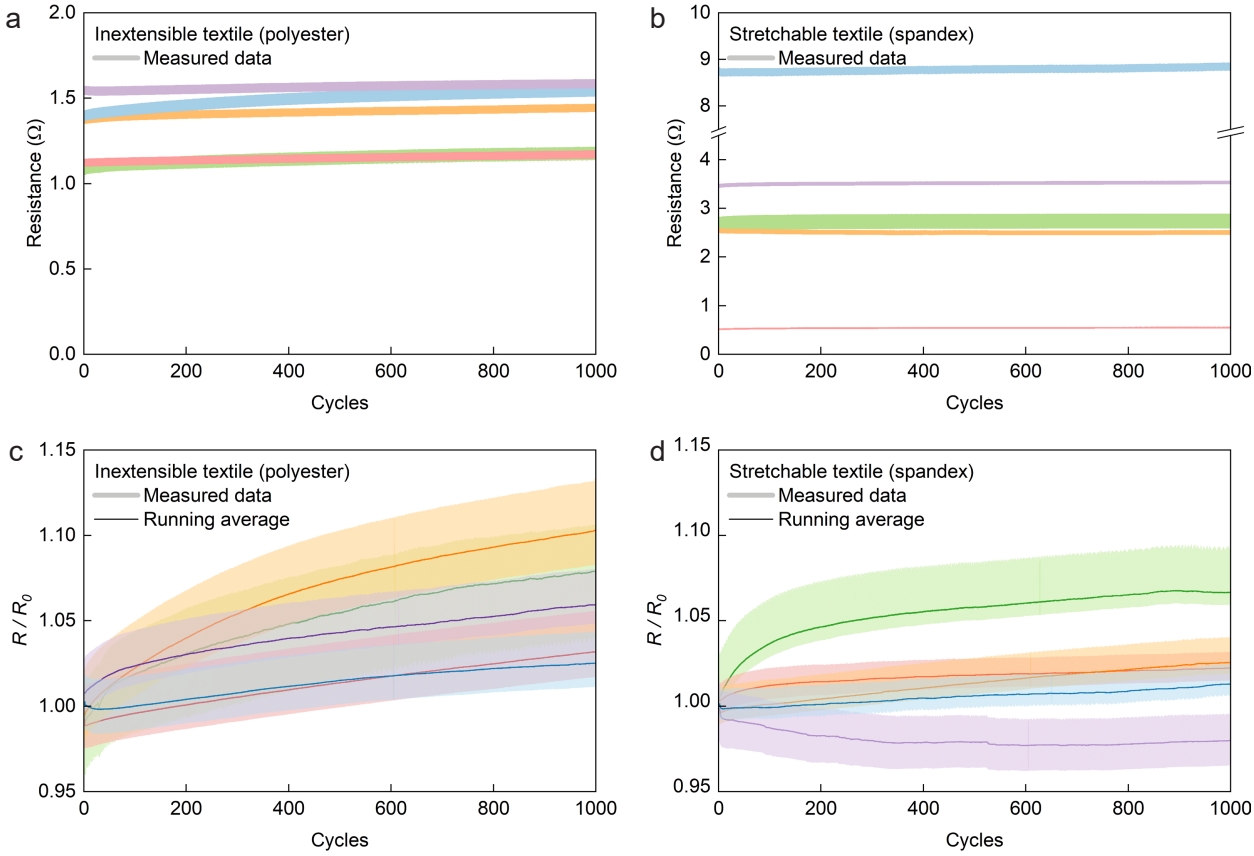

Fig. S7 Cyclic folding of textile-integrated LM wire. (a) Measured resistance of LM wires on polyester textiles during cyclic folding. $n = 5$. (b) Measured resistance of LM wires on spandex textiles during cyclic folding. $n = 5$. (c) Normalized resistance for same data as in *A*. Shaded region represents cycle-to-cycle oscillation, line calculated by a 2-cycle running average. $n = 5$. (d) Normalized resistance for same data as in *B*. Shaded region represents cycle-to-cycle oscillation, line calculated by a 2-cycle running average. $n = 5$.

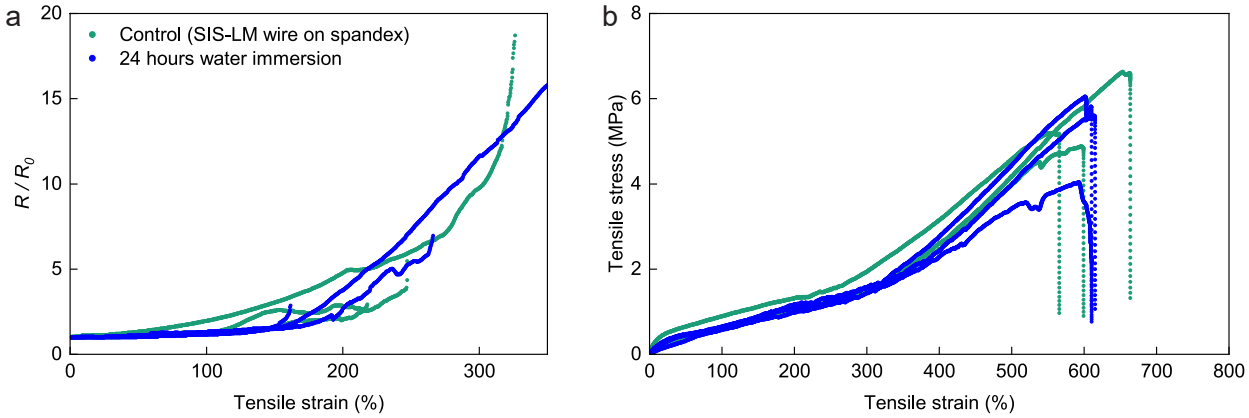

Fig. S8 Electromechanical properties of SIS-LM wire on spandex after 24 hours of immersion in water. (a) Normalized resistance of water-aged specimens plotted alongside control specimens which were not immersed in water. (b) Tensile mechanical response of water-aged and control specimens.

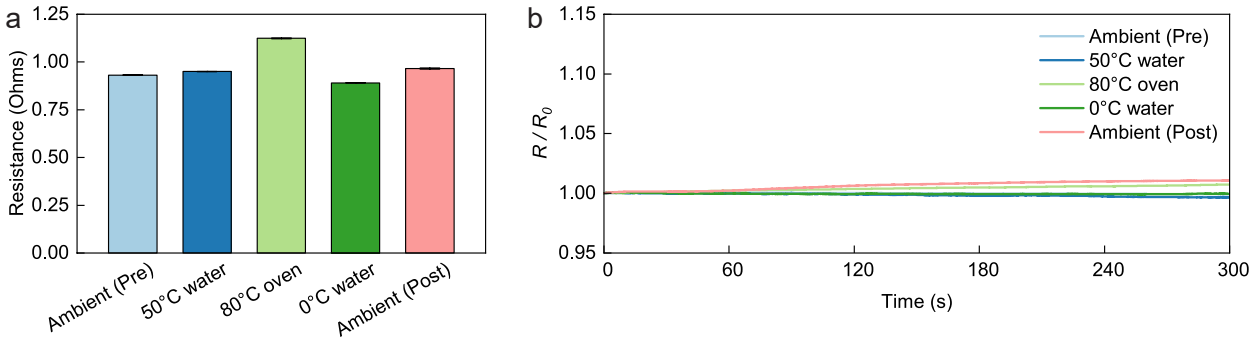

Fig. S9 Temperature reliability of SIS-LM wire on spandex. (a) Resistance of LM wire under ambient air, 0 and 50°C water, 80°C air, and ambient air again after all temperature exposures. (b) Stable normalized resistance over time during various elevated and reduced temperature exposures.

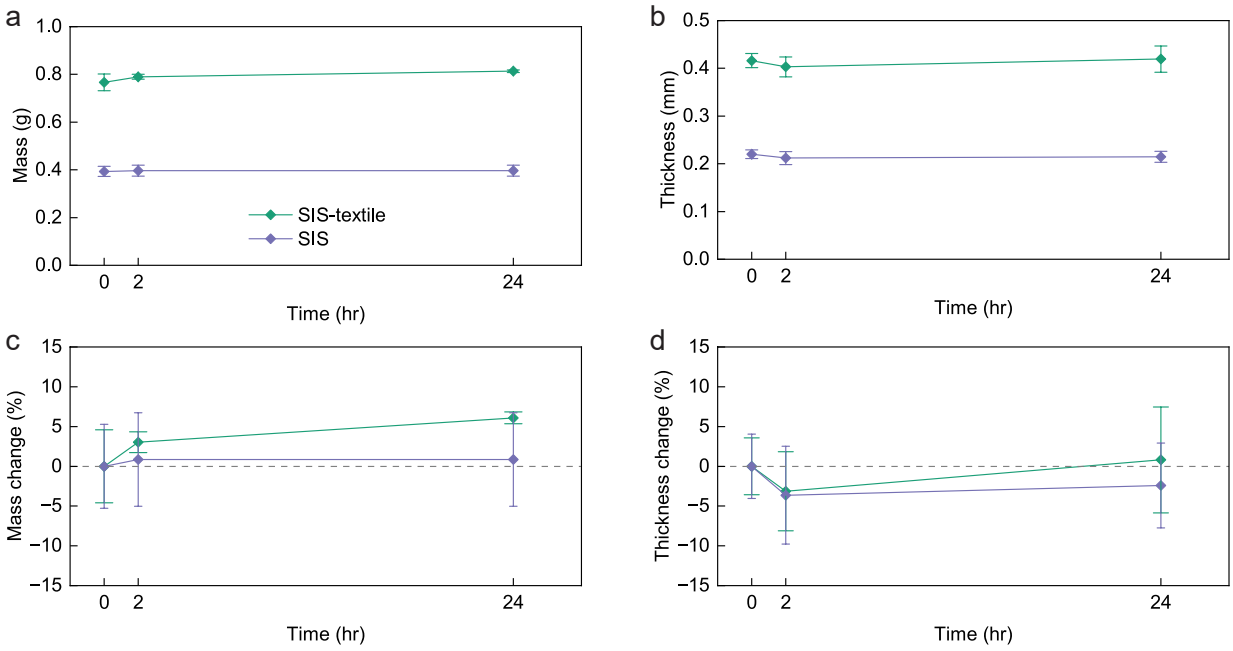

Fig. S10 Water absorption of SIS and textile, conducted following ASTM D570. (a) Mass of either SIS sheets or SIS sheets integrated with textiles measured at 0, 2, and 24 hours of immersion in DI water. (b) Thickness measured at 0, 2, and 24 hours of immersion in DI water. (c) Relative change in mass for data presented in (a). (d) Relative change in thickness for data in (b). Error bars represent 1 s.d. for $n = 3$ measurements.

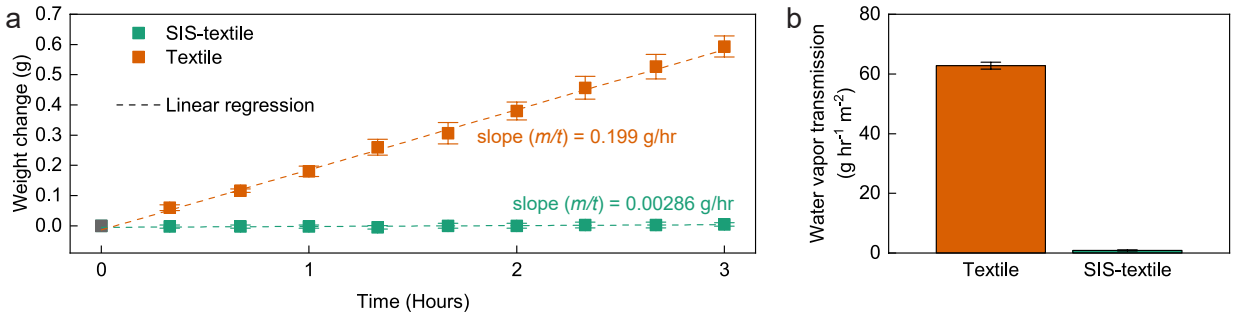

Fig. S11 Water vapor transmission of textile and SIS-textile, conducted following ASTM E96. A cup (Thwing-Albert 68-3000) of DI water was sealed with either a textile or SIS-textile layer covering the top and placed in a fume hood. The assembly was weighed every 20 minutes to track the evaporation of water through the material. (a) Change in measured weight over time for textile and SIS-textile test assemblies. Error bars represent 1 s.d. for $n = 3$ measurements. (b) Water vapor transmission (WVT), calculated through $WVT = m/tA$, where m/t is the mass lost over time, found through a linear regression of the data in (a), and A is the cup mouth area (0.003167 m^2).

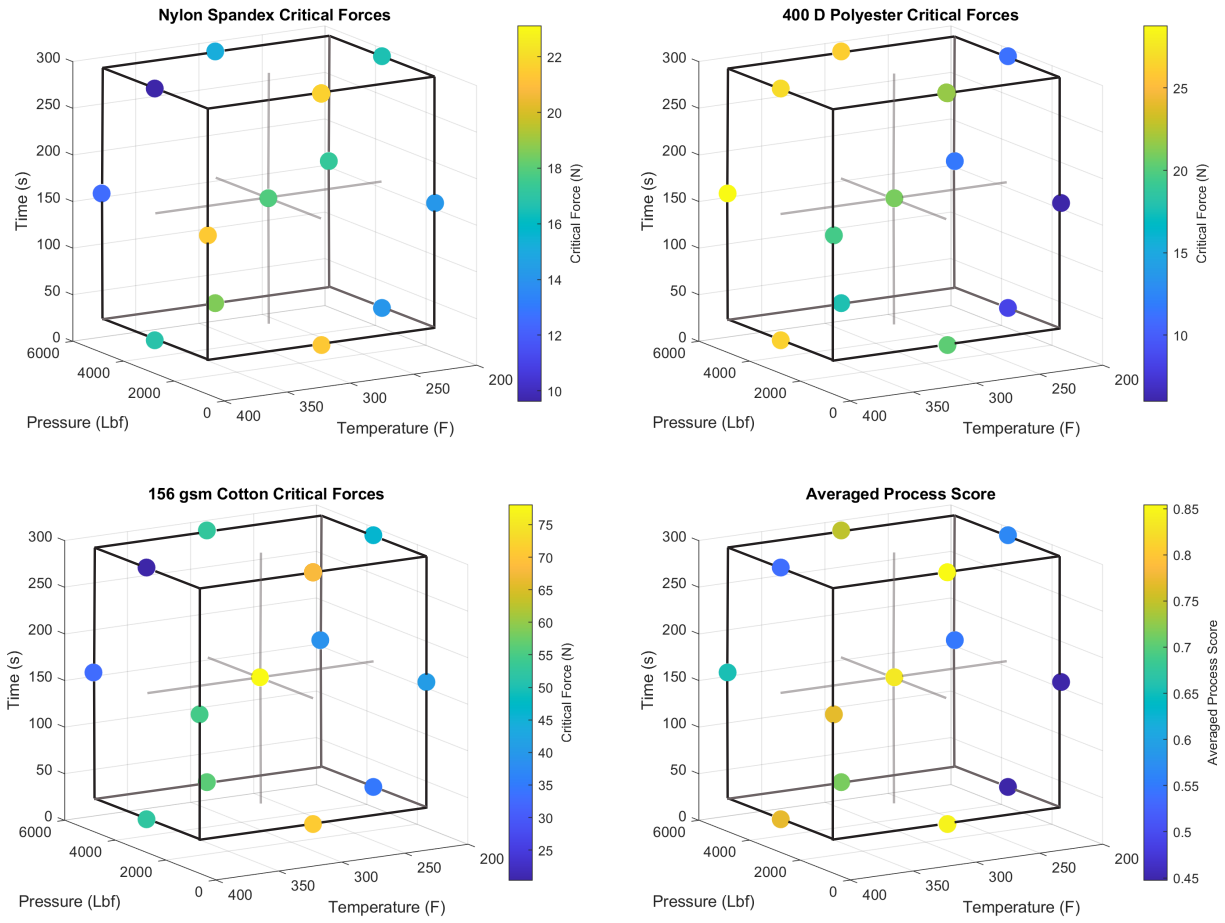

Fig. S12 Box Behnken analysis of temperature, pressure, and time parameters for optimization of adhesion.